Robotica (2015) volume 33, pp. 920–932. © Cambridge University Press 2014
doi:10.1017/S0263574714000599

A simple and novel helical drive in-pipe robot

Yonghua Chen†*, Qingyou Liu‡ and Tao Ren‡

†*Department of Mechanical Engineering, University of Hong Kong, Hong Kong*
‡*State Key Laboratory of Oil and Gas Reservoir Geology and Exploitation & School of Mechatronic Engineering,Southwest Petroleum University, Sichuan Province, P.R. China*

(Accepted February 13, 2014. First published online: March 21, 2014)

SUMMARY
Pipeline grids of various size and material are pervasive in today's modern society. The frequent inspection and maintenance of such pipeline grids have presented a tremendous challenge. It is advocated that only advanced robot design embedded with intelligent electronics and control algorithms could perform the job. Given the ever increasing demands for intelligent in-pipe robots, various in-pipe drive mechanisms have been reported. One of the simplest is helical wheel drives that have only one degree of freedom. All previously reported in-pipe helical drives are based on independent passive wheels that are tilted an angle. One of the major problems of current helical wheel drives is their unstable traction force. In this paper, instead of allowing the wheels to rotate independently, they are synchronized by adding a timing belt. This small change will result in significant improvement which will be highlighted in this paper. In the proposed driving method, tracking force is analyzed together with a comprehensive set of traction force measurement experiments. Both analysis and experiments have shown that the proposed mechanism has great potential for in-pipe robot drive design.

KEYWORDS: In-pipe robot; Helical drive; Traction force; Track drive; Timing belt.

1. Introduction

Today, there are wide spread use of pipelines for transporting or delivering gas, water, oil, or other fluidic materials. Such pipe lines are inside our houses (or high rise towers), underground, below the sea bed, or through a mountain. Over a period of operation, various problems may occur inside pipelines due to ageing, corrosion, and external impact. Some of the most common failure modes are corrosion, pitting, crack, dents, ovalization or deformation. In order to extend the life expectancy of pipelines and to avoid unexpected accidents caused by such failure modes, regular inspection inside pipeline grid is practiced by most companies involved in gas, water, or oil supplies. Whenever a problem is spotted, rehabilitation or repair jobs must be done inside pipes. Due to the small space, long distance, and hazardous environment inside pipes, the application of robots for such jobs is considered as the most attractive solution.

Because of the importance of pipeline transported substance (expensive, poisonous, or necessity), the variety of pipeline application background (Pipelines may vary in terms of material, size, grid complexity, and applications), and the massive use of pipelines for gas and fluidic material transportation, a lot of research works have been conducted and reported on developing methods and machines to carry out various jobs inside pipelines. One of the most popular methods for in-pipe task is to develop in-pipe robots.[1,2] Many types of robot design have been reported. It is impossible to design an in-pipe robot that is superior to others for all types of pipelines or applications. According to Loh *et al.*,[1] currently reported in-pipe robots can be classified into seven types based on differences in the robot driving mechanism design. The seven types are (a) pig type,[3] (b) wheel type,[4] (c) caterpillar type,[5] (d) wall-press type,[6] (e) walking type,[7] (f) inchworm type,[8,9] and (g) screw type,[10]. Each type of design has some merits over others in certain aspects. The actual design adopted may depend on

* Corresponding author. E-mail: yhchen@hku.hk

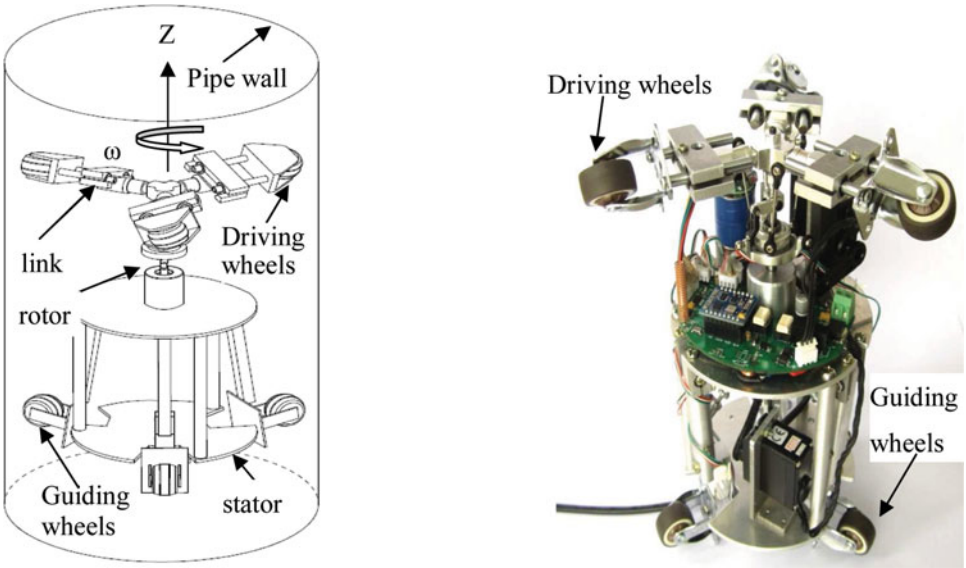

(a) A conceptual design (b) a physical prototype

Fig. 1. A typical helical in-pipe robot design.

the task space of the required applications. More recently, a hybrid design based on type (d) and (g) has been reported by Horodinal *et al.*[11] and Kakogawa *et al.*[12] The hybrid design is basically a wall pressing helical type which is simple in electro-mechanical design, yet can provide adequate mobility within a relatively small space constrained by pipes.

Due to the simplicity of the mechanical structure and the electrical drive, wall-pressing helical drive based robots have been actively researched. Horodinca and Doroftei *et al.* reported a simple structural design of a wall-pressing helical in-pipe robot.[11] No analysis about the characteristics of the design was provided. Kakogawa and Ma have done a great deal of work on the detailed design of a helical drive in-pipe robot in the past a few years. In a paper published in 2010 by Kakogawa and Ma, motion analysis of a helical drive robot was reported. The velocity computation of passive wheels in three coordinate axes x, y and z is detailed.[12] They further reported a method to calculate the optimal spring stiffness of the tilted driving wheels so that the robot could provide enough torque to turn around a bend.[13,14] Apart from being used for in-pipe traction, helical drives are also used as modular units to build more complicated snake-like robot that can move in open fields mimicking a snake's motion.[15]

All previous reports on helical drive in-pipe robots have similar design as shown in Figs. 1(a) and (b). The driving wheels are tilted to move in a helical path inside a pipe. There are variations on the number of driving wheels in previous studies. The pressing force between the wheel and the pipe wall is provided by either using a simple mechanism or a spring as shown in Fig. 2(a). Each wheel is allowed a certain range of radial displacement. This feature enables the helical drive robot to move around some bend as shown in Fig. 2(b) or be adaptive (to some degrees) to diameter change of a pipe as shown in Fig. 3.

However, some of the major problems of current helical drives are their small and unstable tractive force and difficulties in moving over an obstacle. The small tractive force is because that it is generated by the rolling friction between the driving wheels and the pipe wall. If the tractive force can be generated by sliding friction, a much bigger tractive force can be generated (in general, sliding friction is much bigger than rolling friction). In this research, a small change has been introduced to the helical drive so that the tractive force will be generated by sliding friction as shown in Fig. 4. Instead of using independent passive driving wheels as in previous studies, a timing belt drive as in Fig. 4(a) is used in this research. Each of the pulley is tilted an angle so that a helical path can be formed while moving inside a pipe. Figure 4(b) is the simple design concept based on which a physical prototype will be built for experimental studies. In Fig. 4(b), the friction generated from the contact between the belt drive and the pipe wall is sliding friction.

https://doi.org/10.1017/S0263574714000599 Published online by Cambridge University Press

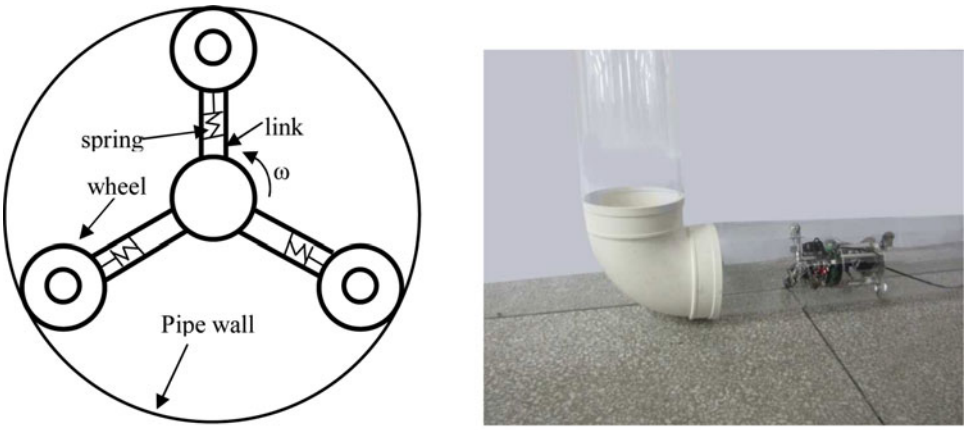

(a) Features of the link design (b) moving inside a pipe

Fig. 2. Features of a helical drive robot.

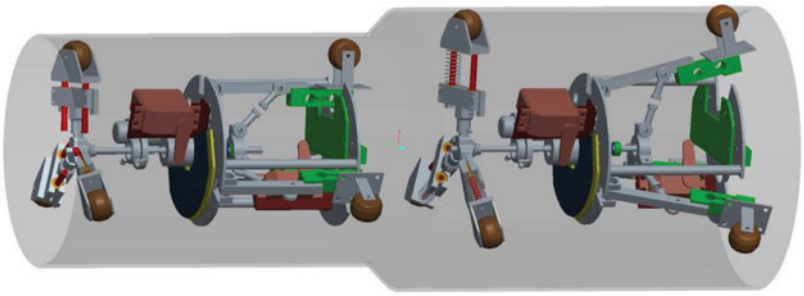

Fig. 3. Robot adaptive to pipe diameter change.

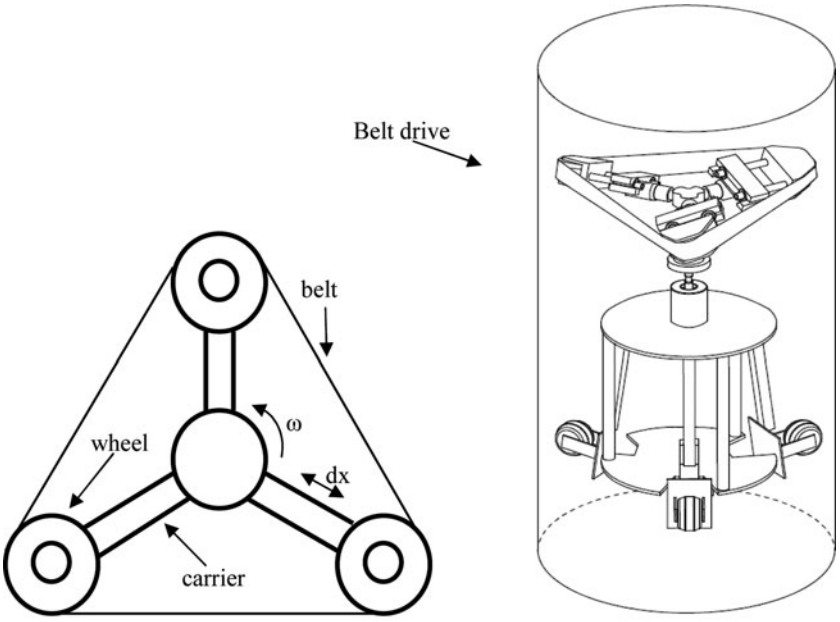

(a) The belt drive (b) The conceptual robot design

Fig. 4. Design concept of a belt drive in-pipe robot.

https://doi.org/10.1017/S0263574714000599 Published online by Cambridge University Press

(a) Teethed elastic belt (b) Flat rubber belt

Fig. 5. Belts used for the wheels.

A fundamental change of the helical drive by adding a belt is that the helical wheel drive shown in Fig. 1 is changed from a passive drive to a positive drive. In Fig. 1(b), when the motor is turned on, the three driving wheels will not rotate against their respective axis. This is equivalent to the none-driving wheels of a two wheel drive car. For the driving wheels shown in Fig. 1(b), only when the wheels are forced against the pipe wall, they will rotate and generate tractive force. Now a belt is added to the three wheels as shown in Fig. 4. This simple modification will turn the passive drive into a positive drive because when the motor is turned on, the three wheels will rotate, and at the same time, the belt will rotate as well. That is, even without contact with the pipe wall, the belt and the wheels will rotate when the motor is turned on. This is equivalent to the driving wheels of a car.

When selecting a belt for the drive, two possible types can be considered, a teethed elastic belt as in Fig. 5(a) or a flat rubber belt as in Fig. 5(b). Since the main intension of the drive is to provide traction, thus the teeth meshing accuracy between the belt and the pulley is not important. In fact, the clearance between the mating teeth is big (in this research, the clearance is around 1mm). This clearance allows the elongation of the belt within a range so that the drive can be adaptive to certain range of pipe radius change. For the case of a flat rubber belt as in Fig. 5(b), since there is a pressing force between the teethed pulley and the belt, the rubber belt will deform thus form a teethed belt. The elasticity of the belt allows the drive to be adaptive to certain range of pipe radius change.

2. Great Improvement from Simple Design Innovation

In this research, instead of using independent tilted wheels for the helical drive robot, a belt is added to the tilted wheels as shown in Fig. 4 so that the rotations of the wheels are synchronized. This minor design innovation results in significant differences in the driving mechanism and may greatly improve the traction capability of the in-pipe robot. In fact, the proposed belt drive can be thought of as a planetary gearing system with a flexible ring gear (the belt). The major differences before and after the design change are summarized below.

(1) With the addition of a belt, the original passive drive is turned into a positive drive. Positive drives are known for much larger traction and predictability compared to passive drives.
(2) The original passive wheel drive is changed to a track drive which is known for large traction force and drive stability compared to a passive wheel drive.[16]
(3) The traction force is generated due to rolling friction in the original passive wheel drive yet it is generated by sliding friction in the belt drive design. In general, sliding friction is significantly larger than rolling friction.[17]
(4) The obstacle negotiating capability of the robot is increased using the belt drive.

The first three features listed above are obvious. As for the fourth feature, even though it has been proved experimentally by using a physical prototype, nevertheless, it will be more helpful to provide a simple theoretic analysis here so that a comparison can be made more easily. For a wheel drive, the obstacle negotiating capability is dependent on the wheel radius. The larger the radius is, the better

https://doi.org/10.1017/S0263574714000599 Published online by Cambridge University Press

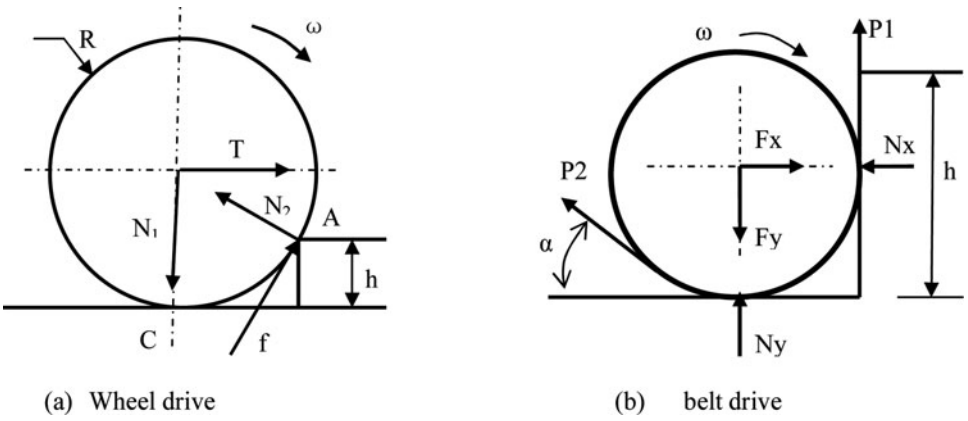

Fig. 6. Obstacle passing capability analysis.

the obstacle negotiating capability will be. When the independent wheels are synchronized by a belt, the wheels and belt system can be treated as forming a single wheel. This wheel is believed to have a better obstacle negotiating capability.

The following is a simple analysis of the obstacle negotiating capability of both drives.

2.1. Wheel drive obstacle passing analysis

When a wheel is about to move over an obstacle as shown in Fig. 6(a), the normal force and friction at the contact *C* are both *0* (because the wheel will be lifted up when climb over the obstacle). Figure 6(a) shows the force analysis of the wheel when it is moving over a simplified obstacle with a height of *h*. To pass over the obstacle, the moment around point *A* must be greater than zero, that is

$$\sum M(A) \geq 0 \tag{1}$$

or

$$T(R-h) \geq N_1\sqrt{R^2-(R-h)^2} \tag{2}$$

Solve Eq. (2) for h we have

$$h \leq R\left(1-\frac{N_1}{\sqrt{T^2-N_1^2}}\right) \tag{3}$$

Where T is the traction force, N_1 is the normal force at the wheel hub, N_2 is the reaction force at the pivot point A, f is the friction at contact A, R is the radius of the wheel, and h is the height of the obstacle. It can be seen from Eq. (3) that the obstacle height h is always smaller than the wheel radius R. In another word, the wheel drive can never pass an obstacle whose height is greater than the wheel's radius. Apart from the wheel radius constraint, the obstacle height h should also be smaller than the allowed radial displacement dx of the wheels, that is

$$dx \geq h \tag{4}$$

2.2. Belt driving obstacle passing analysis

For the belt drive, the drive system can be treated as a single wheel thus its obstacle negotiating capability will be much better. This can also be re-enforced by the facts that many field vehicles use track drives instead of wheel drives.

Figure 6 (b) shows the force analysis of a pulley in climbing over an obstacle. When the pulley is lifted up a bit, the normal force N_y is zero.

https://doi.org/10.1017/S0263574714000599 Published online by Cambridge University Press

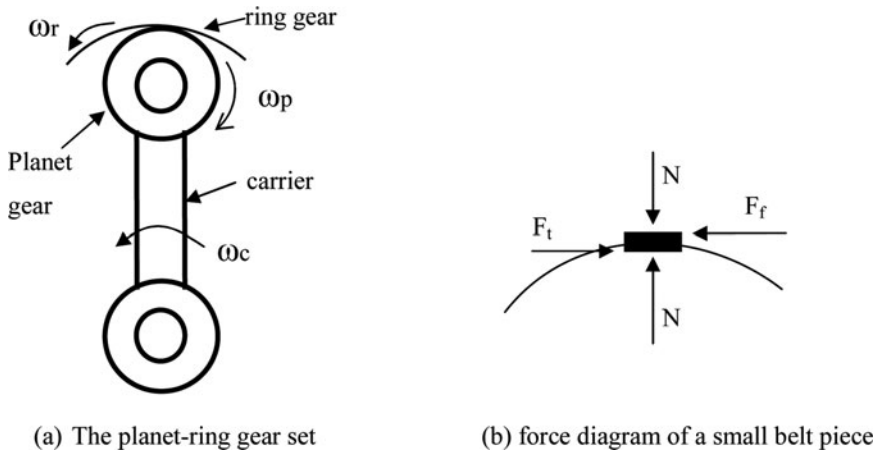

(a) The planet-ring gear set (b) force diagram of a small belt piece

Fig. 7. The planet-ring gear set.

In order to move over the obstacle, the following two conditions must be met. First, the radial displacement of the pulley dx (as in Fig 4(a)) must be greater than or equal to the height of the obstacle h, that is, Eq. (4) is equally applied to the belt drive. Secondly, the vertical force from the belt must be greater than or equal to F_y. F_y is dependent on the spring displacement d_x and the spring constant k used in the pulley carrier.

$$P_2 \sin\alpha + P_1 \geq F_y \quad \text{or} \quad P_2 \sin\alpha + P_1 \geq kd_x. \tag{5}$$

From this analysis, it can be seen that the obstacle climbing capability of the belt drive design is no longer dependent on the wheel radius. In fact, from Fig. 6, it is intuitive that the belt drive has a better obstacle climbing capability as there are two lifting forces for the pulley, yet no such forces in the case of passive wheel drive shown in Fig. 6(a).

3. Traction Analysis

A helical drive in-pipe robot normally has two major parts, a stator and a rotor as shown in Fig. 1. Wheels are installed on both the stator and rotor. In all previous studies, wheels will rotate independently and passively as the rotator rotates. The tractive force is provided by the wheels on the rotor which have a tilted angle. The rolling friction between the wheels and the pipe wall determines the magnitude of the tractive force.

In the proposed belt drive, the traction is mainly due to the sliding friction between the belt and the pipe wall. It is commonly known that the coefficient of rolling resistance is generally much smaller than the coefficient of sliding friction [17].

In analyzing the forces transmitted to the belt in the proposed drive, the belt drive system is considered as a planet-ring gear set where the belt is treated as the ring gear and the pulley as the planet gear as shown in Fig. 7(a). The planet-ring gear set meet the following geometric and kinematic requirements:

$$R_r\omega_r = R_c\omega_c + R_p\omega_p, \tag{6}$$

$$R_r = R_c + R_p, \quad \text{or} \quad R_c = R_r - R_p, \tag{7}$$

where R_r—ring gear radius, R_c—carrier radius, R_p—planet gear radius, ω_r—ring gear angular velocity, ω_c—carrier angular velocity, ω_p—planet gear velocity.

https://doi.org/10.1017/S0263574714000599 Published online by Cambridge University Press

The gear ratio between the ring gear and the planet gear

$$g_{rp} = N_r/N_p = R_r/R_p = T_r/T_p \tag{8}$$

where N_r—teeth number of the ring gear, N_p—teeth number of the planet gear, T_r—torque transmitted by the ring gear, and T_p— torque transmitted by the planet gear.

Divide each term in Eq. (6) by R_p, we have

$$g_{rp}\omega_r = \omega_p + (R_c/R_p)\omega_c \tag{9}$$

Substitute (7) into (9), we have

$$g_{rp}\omega_r = \omega_p + (g_{rp} - 1)\omega_c \tag{10}$$

When the pressure between the timing belt and the pipe wall is big enough, the belt will not slip, that is $\omega_r = 0$, then Eq. (10) becomes

$$\omega_p = (1 - g_{rp})\omega_c \tag{11}$$

The power P transmitted by the planet—ring gear set,

$$P = |T_c\ \omega_c| + \left|T_p\ \omega_p\right| \tag{12}$$

Since angular velocity may have negative value, the absolute value is used here. Torques transmitted by the carrier T_c and the planet T_p have the following relationship

$$T_c = T_p(R_c/R_p) \quad \text{or} \quad T_c = g_{cp}T_p \tag{13}$$

where $g_{cp} = R_c / R_p$

Substitute (13) into (12), we have

$$P = g_{cp}T_p\omega_c + |T_p\omega_p| \tag{14}$$

Substitute (11) into (14),

$$P = g_{cp}T_p\omega_c + |T_p(1 - g_{rp})\omega_c| = T_p\omega_c(g_{cp} + g_{rp} - 1) \tag{15}$$

Since g_{rp} is always greater than one, the term $(1 - g_{rp})$ is changed to $(g_{rp} - 1)$ in Eq. (15).

The torque transmitted by the planet gear can be represented as

$$T_p = P/[\omega_c(g_{cp} + g_{rp} - 1)] \tag{16}$$

Refer to Fig. 7 (b), the tangential force F_t between the planet gear and the ring gear is

$$F_t = T_p/R_p = P/[\omega_c(g_{cp} + g_{rp} - 1)]R_p = P/[\omega_c(R_c + R_r - R_p)] = P/(2R_c\omega_c) \tag{17}$$

Friction between the belt and the pipe wall

$$F_f = N_f \tag{18}$$

Where f is the coefficient of friction.

To make sure that no slippage between the belt and the pipe wall will occur, the friction F_f must be greater than the tangential force F_t, that is,

$$N_f \geq P/(2R_c\omega_c) \tag{19}$$

https://doi.org/10.1017/S0263574714000599 Published online by Cambridge University Press

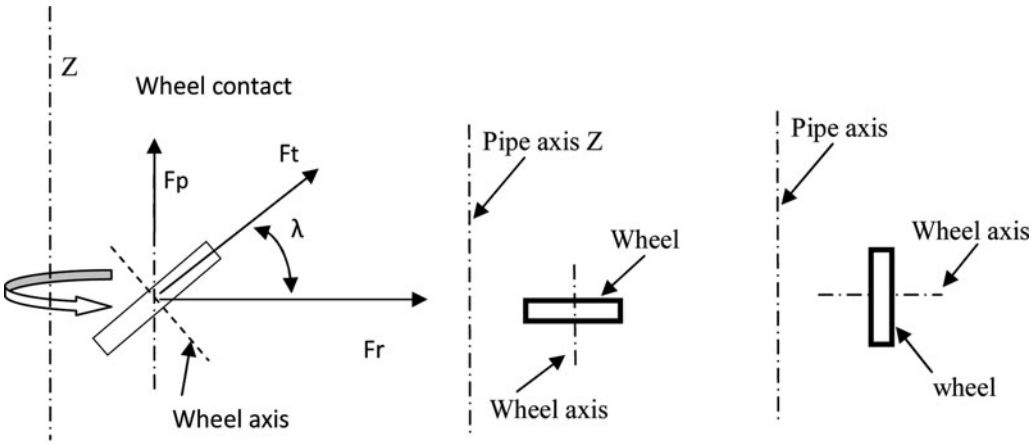

(a) Wheel with a tilt angle (b) Zero wheel tilt angle (c) 90^0 wheel tilt angle

Fig. 8. Forces at the belt contact.

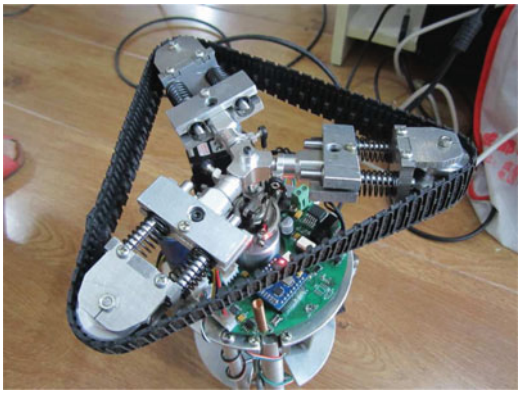

Fig. 9. The prototype in-pipe robot.

Since the pulleys are tilted an angle λ as shown in Fig. 8(a), the actual tractive force along the axial direction (Z direction) should be

$$F_p = [P/(2R_c\,\omega_c)]\sin\lambda \tag{20}$$

Tractive force calculation using Eq. (20) is good when the tilt angle λ is small. As the tilt angle λ increases, the force component along the wheel axis direction will become more dominant. This will reduce the tractive force along the Z direction. In fact, when λ is 0^0 and 90^0 as shown in Figs. 8(b) and (c), the tractive force will be zero.

4. An Experimental Design and Traction Measurement

Gas and liquid transportation pipelines can be very complicated, involving various junctions, branches, and pipe fittings, etc. In order for the proposed robot to be adoptable to more different pipeline environment, the prototype in-pipe robot developed in this research has incorporated a large number of features so that different intelligent control algorithms could be tested at a later stage. For example, the helical angle of the driving wheels can be automatically controlled. A pressure sensor for each of the guiding wheels is installed so that pressure adjustment to the wheels can be done whenever needed. Figure 9 shows the physical prototype of the proposed in-pipe robot. All features of the robot are shown in Fig. 10.

For an in-pipe robot, the tractive capability is very important. Even though, a theoretic analysis of tractive force has been done in the previous section, yet the impact of the wheel axial thrust to

https://doi.org/10.1017/S0263574714000599 Published online by Cambridge University Press

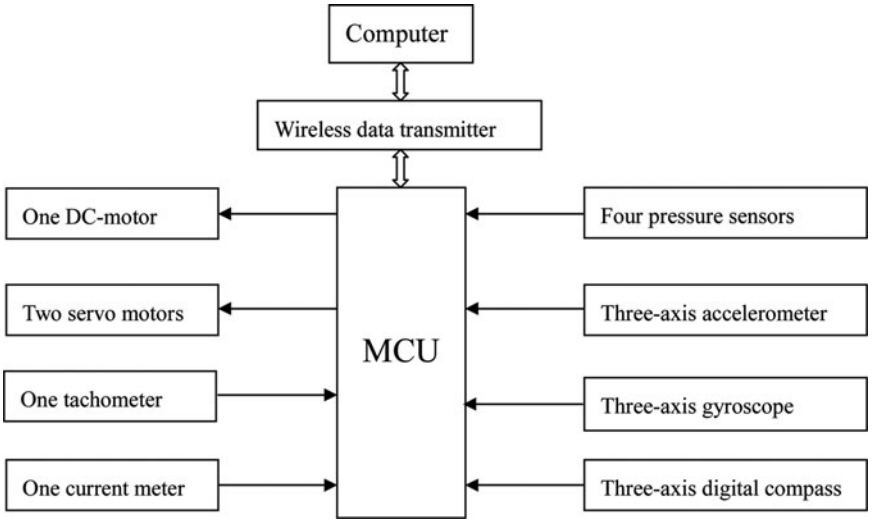

Fig. 10. Diagram showing the features of the prototype in-pipe robot.

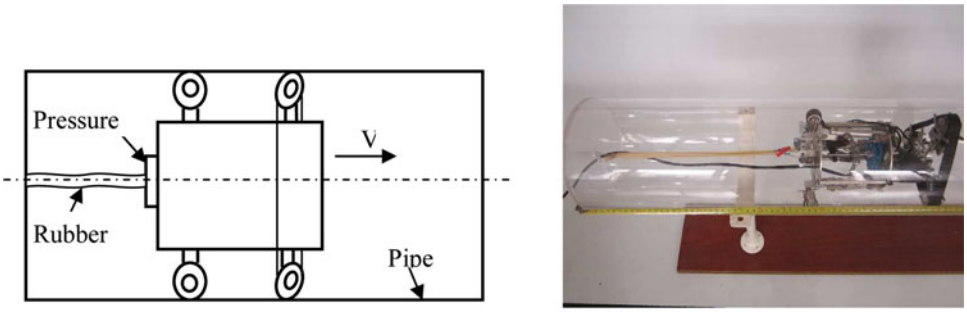

(a) Schematic of the experiments (b) The actual experimental set-up

Fig. 11. Experiments for tractive force measurement.

the tractive force is not easy to be quantitatively expressed. In this research, tractive forces against different wheel tilt angles are measured. These measurements will help to set the right wheel tilt angle so that near maximum tractive force could be obtained.

Figure 11(a) shows the schematic of the experiment. Wheels on the rotor can be tilted an angle through the on-board control system. For a given tilt angle, the rotor is turned on and the robot will move ahead inside a pipe. The longest distance for each tilt angle is recorded. Figure 11(b) shows the actual experiment set-up.

Figures 12(a) to (g) shows the measurements of distance travelled for each wheel tilt angle. The decimal readings of angles are mainly because that the current control software only allows voltage control of motor drive. The conversion from voltage to tilted angle results in decimal points. From Fig. 12(h), it can be seen that when the wheel tilt angle is between 24.9^0 and 28^0, the robot traveling distance will reach the maximum. Further increasing the wheel tilt angle, say to 34.4^0, the maximum traveled distance will decrease. This is mainly because that the engagement between the wheel and the belt deteriorate as the tilt angle increases. It is desirable to develop a mathematical model to accurately describe the influences of the tilt angle on the tractive force. This obviously needs further research.

For each wheel tilt angle, the tractive forces are measured three times as shown in Fig. 13 where the vertical axis presents the recorded force, and the horizontal axis is the time (in second) traveled. Based on the measurement data, a nominal traction force for each wheel tilting angle is extracted. The nominal force is got based on the inequality $dF/dt < \varepsilon$, where$\varepsilon$is a small number. In this experiment, $\varepsilon$was set to *0*. That is, the nominal force is got at the location where a force drop is

https://doi.org/10.1017/S0263574714000599 Published online by Cambridge University Press

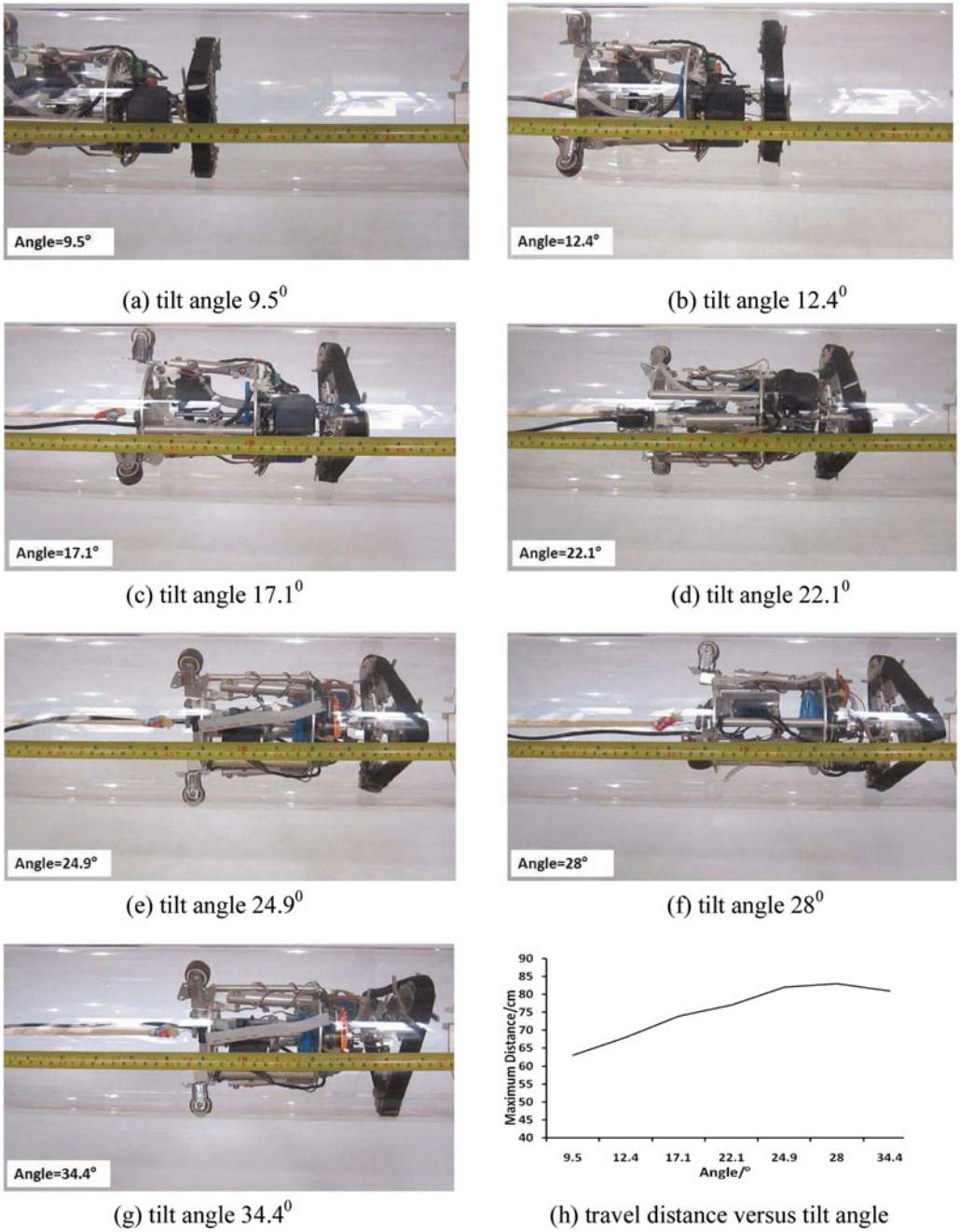

Fig. 12. Maximum travel distance vs. tilt angles.

recorded. Figure 13(h) shows the relationship of maximum traction force against the wheel tilt angle. Again, the maximum traction force occurs when the wheel tilt angle is between 24.9^0 and 28^0. This experimental finding will help to set the wheels to the right tilt angle so that maximum tractive force could be obtained.

To compare the traction of the belt drive and the wheel based drive, the prototype as shown in Fig. 1(b) is also used to do a traction experiment. Only wheel tilt angle of 16.9^0 is conducted. Fig. 14 shows the results. It can be seen that the tractive force has very large fluctuation. In Fig. 13(c), the belt drive has similar tilt angle, yet the tractive force grows steadily and smoothly.

https://doi.org/10.1017/S0263574714000599 Published online by Cambridge University Press

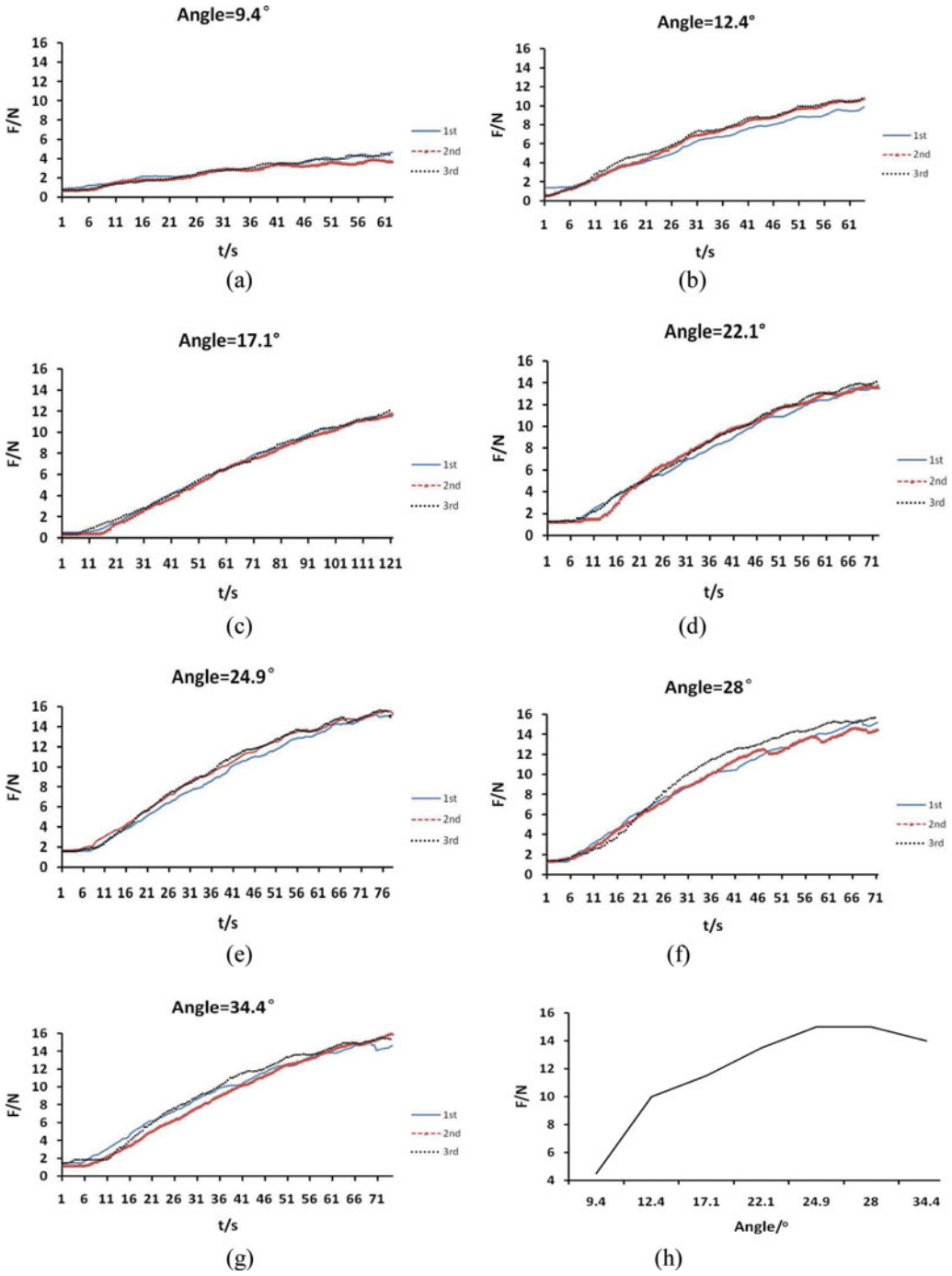

Fig. 13. Maximum tractive force vs. tilt angles.

5. Discussion and Conclusions

A simple and novel helical drive in-pipe robot has been proposed and prototyped. Features such as obstacle passing capability and tractive force have been analyzed. A comprehensive set of experiments aimed at finding the optimum tractive force with respect to the wheel tilting angle have been conducted. It is found that when the wheel tilting angle is between 24.9° and 28°, the tractive force will reach the maximum for the prototype robot.

However, the design of the prototype is not optimized. For example, the pulleys for the belt drive are currently placed on the same plane and tilted as in Fig. 15(a). This causes belt twist and results in frequent belt ripping off the pulleys.

https://doi.org/10.1017/S0263574714000599 Published online by Cambridge University Press

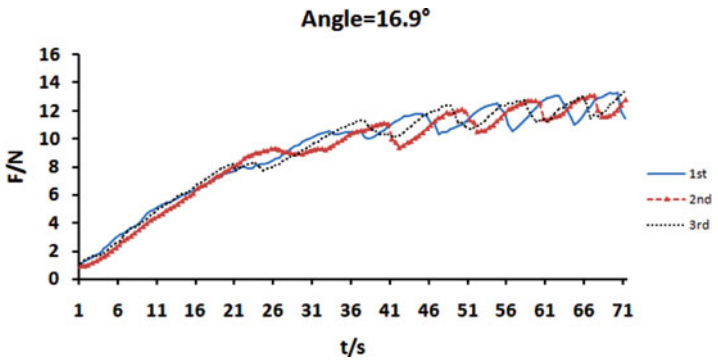

Fig. 14. A sample measurement for wheel based in-pipe robot.

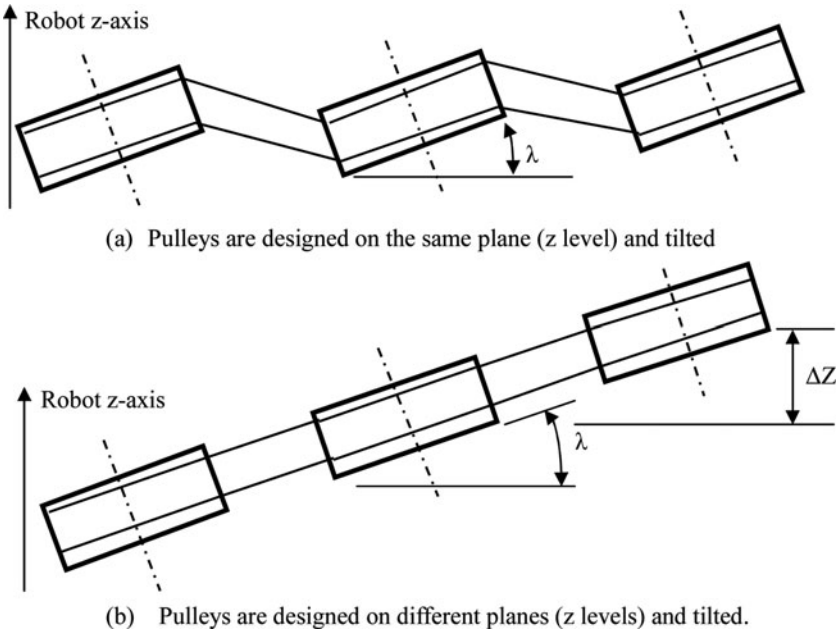

Fig. 15. Two options in pulley design.

An alternative pulley design might be as in Fig. 15(b) where the pulleys are tilted in line so that the belt will not have so many twists. This may result in a better belt drive thus provide smoother tractive force. In future research, the pulley design in Fig. 15(b) will be tested.

The belt drive itself is not optimized either. Ideally, a timing belt is preferred. However, since the timing belt will be elongated when installed onto the pulleys, the accuracy of meshing between the pulley and the belt becomes a problem. This problem may partly be overcome by replacing the timing belt by a plane rubber belt. In all, a lot remain to be studied in designing an appropriate belt drive system for the in-pipe robot.

Acknowledgements

The authors are grateful for the support of Sichuan Province of China Science and Technology Support Program (project code: 14ZC1895). Comments from the reviewers are greatly appreciated.

References

1. S. Roh and H. C. Choi, "Differential-drive in-pipe robot for moving inside urban gas pipelines," *IEEE Trans. Robot.* **21**(1), 1–17 (2005).

https://doi.org/10.1017/S0263574714000599 Published online by Cambridge University Press

2. Y. J. kim, K. H. Yoon and Y. K. Park, "Development of the Inpipe Robot for Various Size," *Proceedings of the IEEE/ASME International Conference on Advanced Intelligent Mechatronics*, Singapore (2009) pp.1745–1749.
3. J. Okamoto, J. C. Adamowski, M. S. G. Tsuzuki, F. Buiochi and C. S. Camerini, "Autonomous system for oil pipeline inspection," *Mechatronics* **9**, 731–743 (1999).
4. J. K. Ong, D. Kerr and K. Bouazza-Marouf, "Design of a Semi-Autonomous Modular Robotic Vehicle for Gas Pipeline Inspection," *Proceedings of the Institution of Mechanical Engineers, Part I: Journal of Systems and Control Engineering*, Vol. 217 (2003) pp.109–120.
5. H. T. Roman, B. A. Pellegrino and W. R. Sigrist, "Pipe crawling inspection robot: An overview," *IEEE Trans. Energy Convers.* **8**, 576–583 (1993).
6. S. Nagano and Y. Oka, "Application of In-Pipe Visual Inspection Robot to Piping Internal Surface Lining," *Proceedings of the 5th International Symposium on Robotics in Construction*, Japan (1988) pp. 897–906.
7. F. Pfeiffer, T. Robmann and K. Loffer, "Control of a Tube Crawling Machine," *Proceedings of the International Conference on Control of Oscillations and Chaos*, Russia, Vol. 3 (2000) pp. 586–591.
8. A. M. Bertetto and M. Ruggiu, "In-pipe inch-Worm Pneumatic Flexible Robot," *Proceedings of the IEEE/ASME International Conference on Advanced Intelligent Mechatronics*, Italy, Vol. 2 (2001) pp. 1226–1231.
9. J. Qiao, J. Shang and A. Goldenberg, "Development of inchworm in-pipe robot based on self-locking mechanism," *IEEE/ASME Trans. Mechatronics*, Digital Object Identifier 10, 1109/TMECH, (2012).
10. C. Anthierens, A. Ciftci and M. Betemps, "Design of an Electro Pneumatic Micro Robot for In-Pipe Inspection," *Proceedings of the IEEE International Symposium on Industrial Electronics*, Slovenia, Vol. 2 (1999), pp. 968–972.
11. M. Horodinca, I. Doroftei, E. Mignon and A. Preumont, "A Simple Architecture For In-pipe Inspection Robots," *Proceedings of the International Colloquium on Autonomous and Mobile Systems*, Magdeburg, Germany (2002) pp. 61–65.
12. A. Kakogawa and S. Ma, "Mobility of an In-pipe Robot with Screw Drive Mechanism inside Curved Pipes," *Proceedings of the IEEE International Conference on Robotics and Biomimetics*, Tianjin, China (2010) pp. 1530–1535.
13. A. Kakogawa and S. Ma, "Experimental Verification of Analytical Torques Enabling a Screw Drive In-pipe Robot to Pass Through Bend Pipes," *Proceedings of the IEEE International Conference on Robotics and Biomimetics*, Phuket, Thailand (2011) pp. 1742–1747.
14. A. Kakogawa and S. Ma, "Stiffness design of Spring for a screw drive in-pipe robot to pass through curved pipes and vertical straight pipes," *Adv. Robot.* **26**(3–4), 253–276 (2012).
15. H. F. Fukushima, S. Satomura, T. kawai, M. Tanaka, T. Kamegama and F. Matsuno, "Modeling and control of a snake-like robot using the screw-drive mechanism," *IEEE Trans. Robot.* **28**(3), 541–554 (2012).
16. J. Y. Wong, W. Huang, "Wheels vs tracks – A fundamental evaluation from the traction perspective," *J. Terramechanics* **43**, 27–42 (2006).
17. F. P. Bowden and D. Tabor, *The Friction and Lubrication of Solids*, Oxford Classics Series Edition (Oxford University Press, Oxford, 2001).